New Insights into Se/$BiVO_4$ Heterostructure for Photoelectrochemical Water Splitting: A Combined Experimental and DFT Study

Siti Nur Farhana M. Nasir,[†] Habib Ullah,*[,‡] Mehdi Ebadi,[⊥] Asif A. Tahir,[‡] Jagdeep S. Sagu,[§] and Mohd Asri Mat Teridi*[,†]

[†]Solar Energy Research Institute (SERI), National University of Malaysia, 43600 Bangi, Selangor, Malaysia

[‡]Environment and Sustainability Institute (ESI), University of Exeter, Penryn Campus, Penryn, Cornwall TR10 9FE, United Kingdom

[§]Department of Chemistry, Loughborough University, Loughborough, Leicestershire LE11 3TU, United Kingdom

[⊥]Department of Chemistry, Faculty of Sciences, Islamic Azad University-Gorgan Branch, Gorgan, Iran

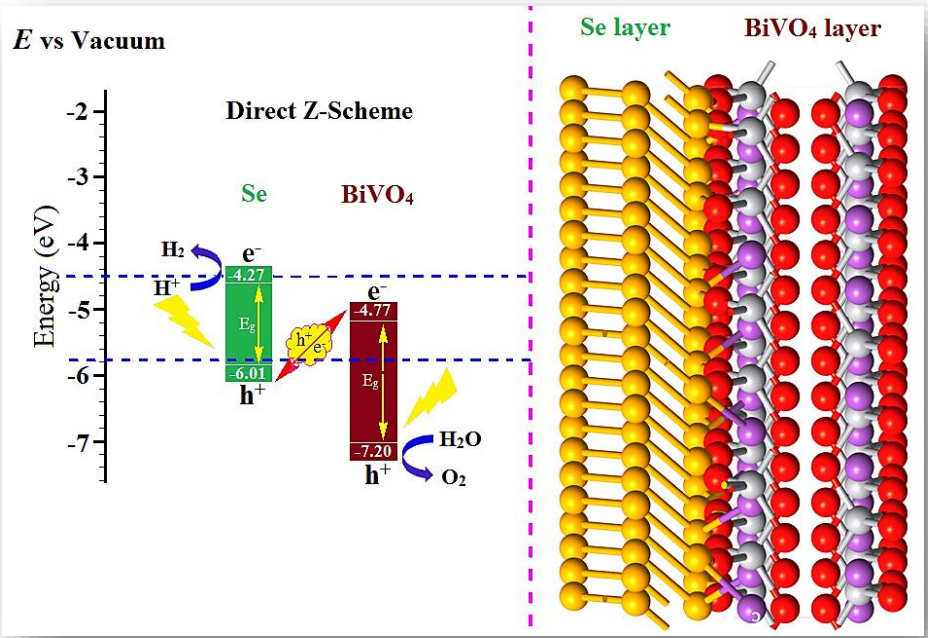

ABSTRACT

Monoclinic clinobisvanite $BiVO_4$ is one of the most promising materials in the field of solar water splitting due to its band gap and suitable VBM position. We have carried out a comprehensive experimental and periodic density functional theory (DFT) simulations of $BiVO_4$ heterojunction with Selenium (Se/$BiVO_4$), to understand the nature of heterojunction. We have also investigated contribution of Se to higher performance by effecting morphology, light absorption and charge transfer properties in heterojunction. Electronic properties simulations of $BiVO_4$ shows that its VBM and CBM are comprised of O 2p and V 3d orbitals, respectively. The Se/$BiVO_4$ heterojunction has boosted the photocurrent density by three fold from 0.7 to 2.2 $mAcm^{-2}$ at 1.3 V *vs*. SCE. The electrochemical impedance and Mott-Schottky analysis consequence favorable charge transfer characteristics which account for the higher performance in Se/$BiVO_4$ compared to the $BiVO_4$ and Se. Finally, spectroscopic, photoelectrochemical and DFT evident that Se makes a direct Z-scheme (band alignments) with $BiVO_4$ where the photoexcited electron of $BiVO_4$ recombine with the VB of Se, consequences electron-hole separation at Se and $BiVO_4$, respectively as a result enhanced photocurrent is obtained.

1. Introduction

Hydrogen has long been identified as one of the most promising energy carriers,[1] which can be easily obtained from renewable resources (water and sunlight) through photoelectrochemical (PEC) water splitting.[1-3] The bottleneck in realizing the concept practically has been the difficulty in identifying stable low-cost semiconductors that meet the thermodynamic and kinetic criteria for photoelectrolysis of water.[1] Suitable materials for PEC should be capable of absorbing maximum photons from visible spectrum of sunlight and function as an effective catalyst for water splitting. Therefore, the semiconductor (electrode) must have band structure with band edge position above and below the redox potential of water, low electron affinity, good photocorrosion stability and bandgap in the range of 1.8-2.2 eV for maximum solar to chemical energy conversion.[4] Since the discovery of Fujishima and Honda,[2] various semiconductors have been investigated to produce hydrogen as a solar fuel from water, using a visible spectrum of sunlight. However, development of suitable and sustainable semiconductor materials as efficient photoelectrode remains a challenge. A metal oxide such as TiO_2 has band edge positions that straddle the standard electrochemical potential of $E°(H^+/H_2)$ and $E°(O_2/H_2O)$, but its large band gap (absorb the UV part of the solar spectrum) accounts for 4 % of the solar irradiance. Although, CdS and CdSe having small band gap and suitable band edge positions but they are not stable under water photooxidation conditions.[5,6] The stable semiconductors such as Fe_2O_3, WO_3, and $BiVO_4$ have been explored for the water splitting application over the last few years.[2,7-12] Among them, Fe_2O_3 is the most widely studied material for H_2 production. However, the conduction band edge of Fe_2O_3 is too low for spontaneous water photoreduction.[13] As a result, complete water splitting with Fe_2O_3 requires large external bias. While WO_3 having a band gap energy of 2.7 eV limits the theoretical solar-to-hydrogen (STH) efficiency to ca. 4.5%.[9] Recently, it has been found that monoclinic clinobisvanite $BiVO_4$ with an ideal band gap with 2.4 eV[14] for water splitting [15] as it can absorb as much as 11 % of the solar spectrum compared to that of the 4 % TiO_2.[16] However, $BiVO_4$

usually shows a low photocatalytic activity owing to poor charge-transport characteristics[9] and weak surface adsorption properties.[17] In addition, many attempts have been made to improve the poor photocatalytic activity of $BiVO_4$ due to its more positive potential in thermodynamic level.[18] Coupling $BiVO_4$ with an oxygen evolution catalyst such as cobalt-phosphate,[18-21] iron oxyhydroxide[22] and cobalt-borate[23] is one of the options. Making a heterojunction between two dissimilar semiconductors is also an effective strategy to improve the electron-hole separation in $BiVO_4$.[2,7-12,18-21,24,25] Heterojunction has great benefit to PEC activities such as broadening the light absorption spectral, suppressing the charge recombination and enhancing charge separation.[25] Representative heterojunctions or band alignments of binary dissimilar semiconductors are shown in Fig 1. Type-I heterojunction (Fig. 1a), an extensively studied PEC water splitting techniques where a narrow band gap semiconductor (Fe_2O_3) is combined with wide band gap semiconductor such as TiO_2.[26] In this combination, a complementary light absorption takes place and photocurrent improves by a consequence of facile electrons and hole transfer from the conduction and valence band of wide band gap semiconductor to small band gap material. In Type-II heterojunction (Fig. 1b), the relatively more negative potential (vs RHE) of the conduction and valence band of a narrow band gap of semiconductor ($BiVO_4$) is beneficial to enable the efficient charge transfer[25] and high photocurrent density. Since the photo-excited electrons in $BiVO_4$ where the conduction band is located at more negative potential can easily transfer an electron to the conduction band of WO_3 that have the conduction band at positive potential (Fig. 1b), responsible for high photocurrent. And as a result, the holes from the valence band of WO_3 can be transferred to the valence band of $BiVO_4$ to oxidize H_2O and generate O_2.[10] In Type III heterojunction, both narrow band gap semiconductors (each having either an ideal VB or CB) are combined to efficiently perform the photoelectrochemical water splitting (Fig 1c). The photogenerated electron at the CB of FeS_2 recombines with a hole at the VB of Sb_2Se_3 and consequences separation of electron and

hole, responsible for high photocatalytic activity.[27] In Type IV band alignments (Fig d), electron-hole pairs separation occurs very easily due to the establishment of a direct Z-scheme in binary semiconductors. Since the photo-excited electrons at CB of wide band gap semiconductor (i.e., $BiVO_4$ or ZnO), located at more positive potential (vs RHE) would recombine with the holes of g-C_3N_4 that have the valence band at a more negative potential (Fig 1d). As a result of the aforementioned recombination, holes from the valence band of ZnO/$BiVO_4$ are transferred into the electrolyte to oxidize $H_2O \rightarrow O_2$, whereas the electrons from the conduction band of g-C_3N_4 are transferred to the counter electrode which enhances the photocurrent.[28] Therefore, a proper band alignment of each semiconductor in all types of heterojunctions is necessary to develop a deeper understanding of the charge transport properties in water splitting process.

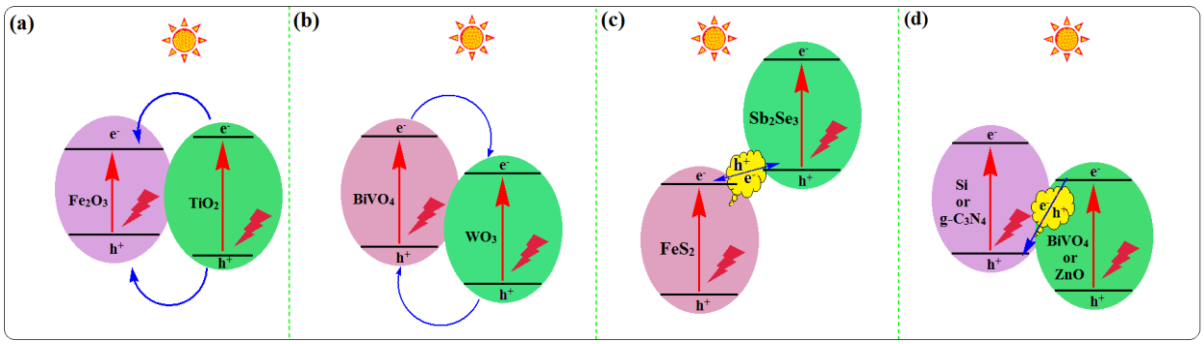

Figure 1: Schematic representation of different band alignments for high PEC performance.

The Type-I and II heterojunction are widely reported compared to Type III and IV, where $BiVO_4$ is mixed with other materials.[9,29,30] From a thermodynamic point of view, the material used in place of g-C_3N_4 must have small band gap energy in case of Type IV heterojunction to favor the electrons excitation process. Graphitic carbon nitride; g-C_3N_4 (E_g = 2.7 eV) and Silicon, Si (E_g =1.1 eV) are the most popular visible light absorbing semiconductor to be paired in various metal oxide for PEC cells.[31-33] The more negative conduction band potential of g-C_3N_4 and Si compared to that of $BiVO_4$, facilitate the photogenerated electrons mobility to the external circuit due to high electron-hole pairs separation. Si-based materials are highly

efficient in the solar cell technology but they are too expensive to be used in PEC water splitting. The cost of a silicon wafer comprises the pure silicon cost, the crystallization cost, and the slicing cost.[34] Also, the fabrication of the Si-based device is more complex as it requires proper handling of fairly fragile Si wafer. These factors lead to a motivation in developing Si-free PEC cell with a potentially good absorber material which can be prepared by easy growth techniques to reduce cost production and achieve high charge transport characteristics in the heterojunction (Type-IV heterojunction).

In this work, we demonstrate improved performance of a $BiVO_4$ (photoanode) through combining with an n-type Selenium (Se), to build band alignments as that of direct Z-scheme (Fig 1d). Se has been extensively studied as a photoabsorber in thin film devices such as solar cells, photocatalyst, xerography, and rectifiers.[35-37] Due to its small band gap, it has high light absorption efficiency[38] and can be combined with $BiVO_4$ to further improve the light harvesting ability. Moreover, Se has low surface states densities, large carrier lifetime[39] and a high conductivity (1×10^{-3} Sm^{-1})[40] which can affect the charge mobility. One disadvantage of Se is that it is more prone to photocorrosion by itself rather than their larger band gap counterparts. Therefore, when Se is coupled with a larger band gap semiconductor (in Type-IV heterojunction), the charge recombination of the photogenerated electron-hole pair can be reduced and also suppresses the Se layer photocorrosion. Since very limited information is available regarding Se-based PEC water splitting, hence, this work is a step forward to provide a new direction to replace a traditional visible-light photoabsorber *i.e* Si with Se. The PEC performance of the Se/$BiVO_4$ heterojunction has been discussed to prove that Se is a promising material to be used as a high-performance visible light absorber in water splitting. Furthermore, periodic density functional (DFT) simulations are also carried out to countercheck the experimental data and elucidate the photocatalytic performance of Se, $BiVO_4$, and Se/$BiVO_4$. The fundamental electronic structure of the monoclinic clinobisvanite

$BiVO_4$ are rarely considered for the water splitting, so, its theoretical investigations along with experimental study might provide rational answers to comprehend the optical and electronic-relationship. Finally, these findings will be useful to get an insight to design an appropriate approach for improved PEC performance.

1. Materials and Methods

2.1. Chemicals

All commercial chemicals were purchased from sigma Aldrich and were used without any further purification. The chemicals used are bismuth nitrate pentahydrate, $Bi(NO_3)_3.5H_2O$, vanadium acetylacetonate, $C_{10}H_{14}O_5V$, sodium selenite, Na_2SeO_3, ethylene glycol, methanol, acetone, and isopropanol.

2.2. Synthesis of Se/$BiVO_4$ photoanodes

Conductive fluorine-doped tin oxides (FTO TEC 18 Ω/cm^2, Pilkington) coated glass were used as substrates. Before the deposition process, all substrates were cleaned with deionized water, followed by acetone and isopropanol for 15 minutes each, respectively in the ultrasonic bath and then dried. A potentiostat/galvanostat modulab solartron analytical was used for electrodeposition. A layer of Se was deposited galvanostatically at -20 mA *vs.* SCE for 90 seconds in an aqueous solution containing 50 mM Na_2SeO_3 with an FTO working electrode, SCE reference electrode, and platinum counter electrode. The as-prepared Se layer was rinsed with deionized water and dried. In next step, the $BiVO_4$ thin film was loaded on Se layer by aerosol-assisted chemical vapor deposition (AACVD). The $BiVO_4$ precursor solution was prepared by dissolving 0.2 M $Bi(NO_3)_3.5H_2O$ in ethylene glycol and 0.2 M $C_{10}H_{14}O_5V$ in methanol as reported in our previous work.[41] The precursor solution was poured into 20 ml round bottom flask which was converted to an aerosol by an ultrasonic dehumidifier and then transferred to the heated zone of a hot plate (where the Se coated FTO sample was placed). The deposition of $BiVO_4$ thin film was conducted for 90 minutes at ~450 ºC in air.

2.3. Computational Methodology

First principle periodic DFT simulations are carried out with the help of Quantum ESPRESSO[42] and the results were visualized with VESTA[43] and virtual nano-lab (vnl 16).[44] The experimentally available crystallographic file of the $BiVO_4$; clinobisvanite structure is used as such which has Hall symmetry space group of -I 4ad with lattice parameters of a = 5.147 Å, b = 5.147 Å, c = 11.7216 Å, and $\gamma = 90°$.[45] The bulk of Se with a space group of $P3_221$ having lattice parameters of a = 4.355 Å, b = 4.355 Å, c = 4.949 Å, $\alpha = 90°$ and $\gamma = 120°$ is used for simulations. The exchange and correlation potential was treated by the Perdew-Zunger, spin-unpolarized local density approximation (LDA). As an input structure for calculations; the 24 atoms unit cell with 2x2x2 supercell having [001] orientation and vacuum space of 10 Å, is taken into account for the periodic boundary condition (PBC) DFT simulations. Mostly, clinobisvanite monoclinic $BiVO_4$ exists in [001] orientation so, that is why the [001] orientation is opted for theoretical simulations to represent the experimental thin film.[46] Moreover, the unreconstructed [001] termination possesses low surface energy and as a result represents the most probable surface termination.[46] A 5x5x1 Monkhorst-Pack k-grid and energy cutoff of 100 Ry is employed for the geometry relaxation and self-consistent (SCF) simulations of $BiVO_4$; consisting of 96 atoms. The Broyden-Fletcher-Goldfarb-Shanno algorithm (BFGS) was used for the structural minimization.[47] A 5x5x5 Monkhorst-Pack k-grid with the same energy cutoff is used for the non-SCF part to get the density of states (DOS) and partial DOS (PDOS). The band structure simulations were performed along the direction of Γ, Z, R, X, and M of the Brillouin zone sampling. The valence electron configurations considered are: $5d^{10}\ 6s^2\ 6p^3$ for Bi; $3p^6\ 3d^3\ 4s^2$ for V; $2s^2\ 2p^4$ for O, and $4s^2\ 4p^4\ 3d^{10}$ for Se atom.

2.4.Characterizations

X-ray diffraction (XRD) measurements were conducted using a (Bruker D8 Advance diffractometer) in the 2θ range from 20 ° to 60 °. The morphologies and elemental mapping of the films were examined by field emission scanning microscopy (FESEM) and energy dispersive X-ray spectroscopy (EDX) on an (FE-SEM SUPRA VP55). Optical characterizations were conducted by a UV-Vis absorption spectrophotometer Perkin Elmer Lambda 950). The PEC measurements were recorded using a potentiostat/galvanostat Autolab PGSTAT 204, connected to the three-electrode configuration in a 0.5 M Na_2SO_4 electrolyte, an SCE (saturated KCl) as the reference electrode and a platinum as the counter electrode in a quartz cell. The chronoamperometry curves of the electrodes were obtained at 0.50 V *vs*. SCE. Electrochemical impedance spectroscopy (EIS) and Nyquist plot were performed using the same experimental setup as the PEC measurements. The frequency was 100 kHz-100 mHz with 0.5 V applied bias under dark and simulated light conditions (light intensity of 100 $mWcm^{-2}$). The illuminated area was 1.0 cm^2 for all experiments and the observed spectra were fitted by using GPES software.

3. Results and discussion

3.1. Structural analysis

The structural phase and purity of the as-synthesized $BiVO_4$ and Se/$BiVO_4$ films are shown in Fig. 2. All the diffraction peaks of Se/$BiVO_4$ were identified to have a monoclinic clinobisvanite $BiVO_4$ which has good agreement with standard JCPDS pattern (00-014-0688). The peaks exhibited from Se thin film was appeared to have a monoclinic Se (JCPDS No. 00-054-0500) (Fig. S1). No impurity phases are observed, which confirms the purity of deposited films. The narrow and sharp peaks from the XRD patterns of all samples indicate high crystalline nature of the films. The peaks of $BiVO_4$ can clearly be seen at 2θ = 28.82°, 30.55°, 34.50°, 35.22°, 39.78°, 42.47°, 46.71°, 47.31°, 50.32° and 53.258° which assigned to the planes of (-121), (040), (200), (002), (211), (051), (240), (042), (202) and (-161) respectively.

These $BiVO_4$ peaks are clearly visible in Se/$BiVO_4$ thin film followed by a small intensity Se peak at (122) while the rest of Se peaks are diminished due to the growth of $BiVO_4$ on top of Se. Meanwhile, the deposition of $BiVO_4$ to form a heterojunction does not cause any changes in the crystal structure of Se and other electronic properties. The crystallite size calculated based on t peaks at (122) for Se and (-121) for $BiVO_4$ in Se/$BiVO_4$ are 838.1 and 369.1 Å, respectively (Fig 2).

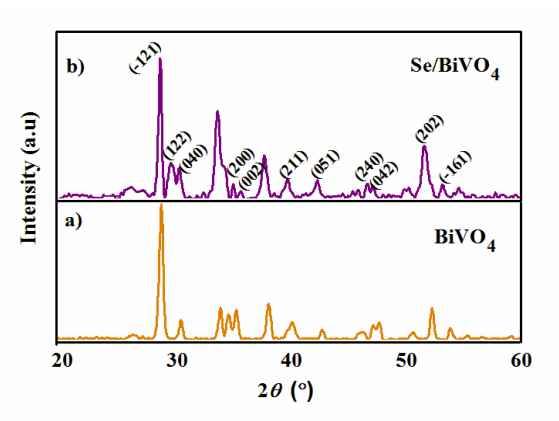

Figure 2: X-ray diffraction patterns of a) $BiVO_4$ and b) Se/$BiVO_4$.

3.2. Morphology

Surface morphology of Se, $BiVO_4$, and Se/$BiVO_4$ thin films are characterised by FESEM analysis which is presented in Fig. 3. The surface morphology of Se film have a dense sponge-like surface with particles diameter in the range of 217-392 nm on average and film thickness is 368 nm (Fig. 3d). The morphology of $BiVO_4$ (Fig. 3b) comprised of a spherical particle bumpy surface with an average particle size and thickness (Fig. 3e) of about 357–680 nm and 570 nm, respectively. The FESEM images of Se/$BiVO_4$ films showed a nanoporous structure with particles size smaller than that of Se and $BiVO_4$ as shown in Fig. 3c. The porous structure beneficial to improve the electrode/electrolyte interfacial area which ultimately increases the movement of the photogenerated charge carriers and reduces the charge recombination rate during the photo-oxidation reactions.[48] The reduction in particle size is consistent with the reduction of the grain size obtained from XRD. The film thickness of Se/$BiVO_4$ is increased

to ~758 nm (Fig. 3f). It is observed that the morphology of Se is denser than that of $BiVO_4$. This feature is suitable for $BiVO_4$ to be deposited on top of the Se layer or in contact with the electrolyte in the heterojunction structure to increase the electrolyte/photoelectrode interfacial area (Fig. 4a).[49] The Se layer is placed on top of the $BiVO_4$ (forming $BiVO_4$/Se heterojunction), along with compact morphology of Se which may obstruct direct contact in $BiVO_4$ layer into the electrolyte, the smaller band gap Se will also hinder light penetration to $BiVO_4$ as well as Se is more prone photocorrosion. (Fig. 4b). As a result, this may not only limit the catalytic reaction but also block some of the light penetration to the $BiVO_4$ film. A similar case is observed in CdS/$BiVO_4$ electrode by Jiang et al.[49] where they compared the influence of the light absorption on CdS/$BiVO_4$ and $BiVO_4$/CdS structures. In addition, the purity and elemental presence of the constituents in the heterojunction (Se/$BiVO_4$) electrode is confirmed through EDX and elemental mapping (Fig. 3g and h). The EDX spectrum shows strong peaks for the Bi, V, O and low level for the Se, while the rest of them are belong to the FTO.

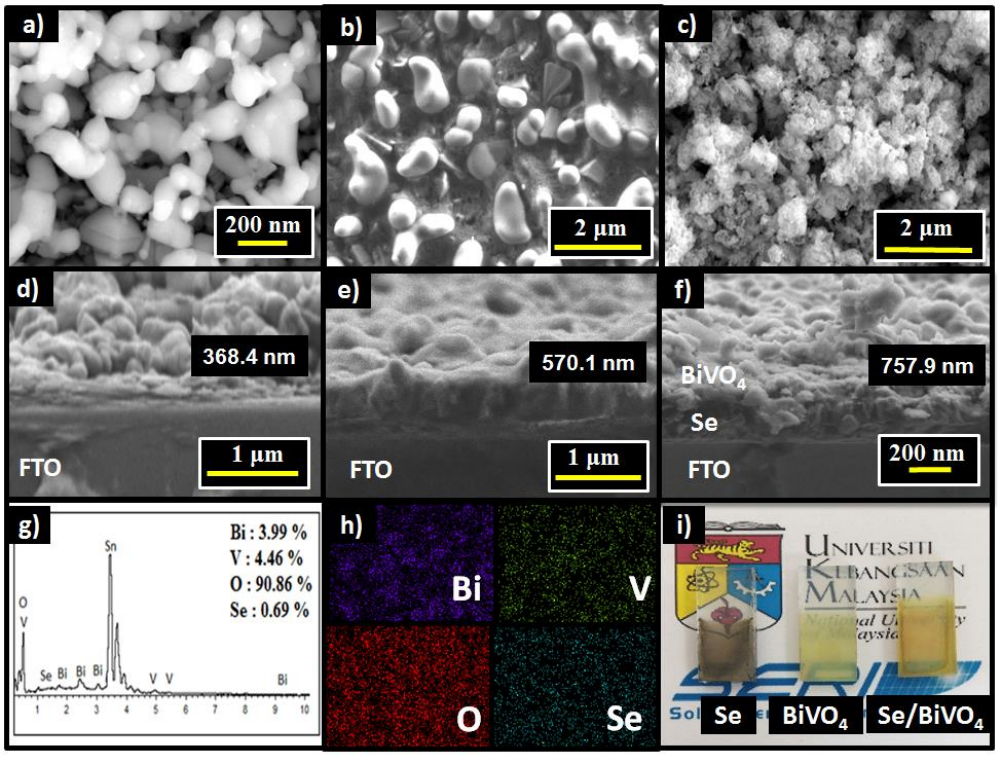

Figure 3: FESEM images and thickness of Se (a) and (d), $BiVO_4$ (b) and (e) and Se/$BiVO_4$ (c) and (f). The EDX spectrum (g) and Elemental mapping (h) of Se/$BiVO_4$, (i) the Se, $BiVO_4$ and Se/$BiVO_4$ samples.

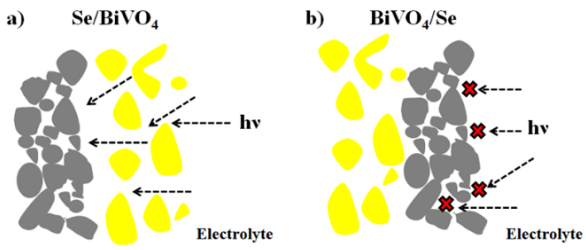

Figure 4: Schematic diagram of a) Se/$BiVO_4$ and b) $BiVO_4$/Se surface structures.

3.3. AFM

The 3D AFM images and surface roughness of Se, $BiVO_4$, and Se/$BiVO_4$ films are shown in Fig. 5 and Table 1. As expected, Se/$BiVO_4$ film showed high surface roughness compared to that Se and $BiVO_4$ films which may be due to the formation of dual layers and thicker films in the heterojunction (Se/$BiVO_4$). Generally, high surface roughness and small grain size can significantly affect the PEC performance as more sites are exposed for the photocatalytic reactions.[50] Moreover, it is believed that films with rough surface enhances the light scattering and improve the light absorption capability.

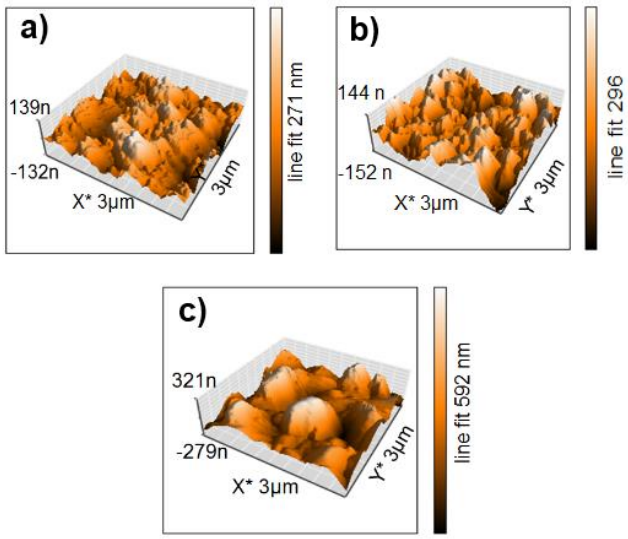

Figure 5: AFM images of (a) Se, (b) $BiVO_4$ and (c) Se/$BiVO_4$.

Table 1: The surface roughness of Se, $BiVO_4$, and Se/$BiVO_4$ thin film photoanodes.

Sample	***Surface roughness (nm)***
Se	32.71
$BiVO_4$	42.85
Se/$BiVO_4$	77.80

3.4. Optical properties

The optical absorption spectra of these films are presented in Fig. 6a, where the low absorption intensity of Se electrode is attributed due to its low thickness. As can be seen in Fig. 3d, the substrate is not fully covered by Se particles and in some part of the electrode, the FTO substrate can clearly be seen, responsible for the light scattering from FTO compared to Se. The absorption intensity of Se/$BiVO_4$ slightly enhanced to shorter wavelength when $BiVO_4$ layer was coated on Se. This enhancement is because of the high absorption intensity of the $BiVO_4$ film, light scattering of porous, rougher surface and thicker film of Se/$BiVO_4$ electrode. Moreover, the Se/$BiVO_4$ thin film is dark yellowish which is almost similar to $BiVO_4$ electrode (see samples shown in Fig. 3i) which suggests that most of the light is absorbed by $BiVO_4$ layer in the heterojunction (Se/$BiVO_4$). Therefore, the Se/$BiVO_4$ thin film electrode is more blue-shifted at a wavelength of ~ 470-500 nm ($BiVO_4$=2.43 eV) compared to ~ 700 nm (Se=1.74 eV). Due to these factors, Se/$BiVO_4$ electrode absorbs more visible light than that of either Se or $BiVO_4$. The optical band gap is calculated according to equation 1.[51]

$$(\alpha hv)^n = A\,(hv - E_g) \qquad (1)$$

Where α is the absorption coefficient, v is the incident light frequency E_g is the band gap and A is constant. n depends on the characteristic of the transition in a semiconductor; for a direct transition, n = 2. The optical band gaps are evaluated from the relation of $(\alpha hv)^2$ *vs*. photo energy (hv). The extrapolations of the Tauc plots on x-intercept give the optical band gap of 2.43 eV for $BiVO_4$ (Fig. S2)[41] and 1.74 eV for Se (Fig. 6) which is also consistent with the recently reported work of Wang et. al.[52]

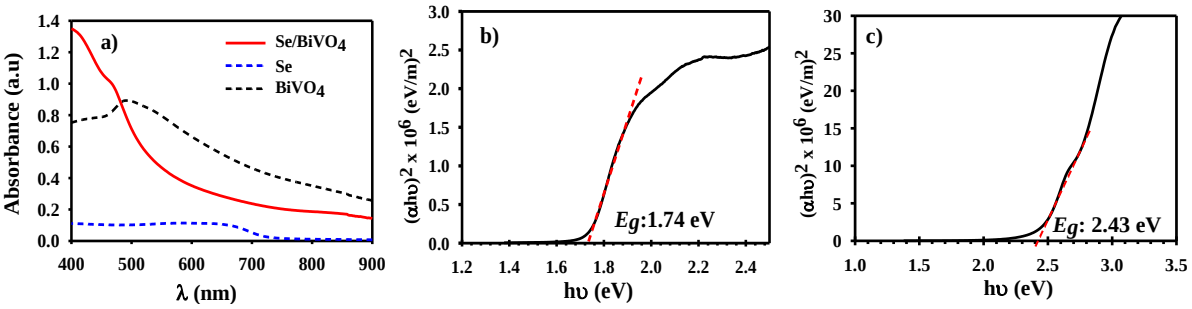

Figure 6: a) UV-vis absorption spectra of the Se, $BiVO_4$ and Se/$BiVO_4$. Tauc plot of b) Se and c) Se/$BiVO_4$ thin films.

3.5. DFT Simulated Electronic and Optical Properties of $BiVO_4$

Basically, $BiVO_4$ exists in three different crystalline polymorphs; orthorhombic pucherite, tetragonal dreyerite, and monoclinic clinobisvanite.[53] The photocatalytic activity and surface reaction is highly dependent on phase and crystal orientation of semiconductor oxide.[54-56] For instance, the tetragonal $BiVO_4$ possesses a band gap of 2.9 eV and mainly absorbs UV light, while the monoclinic clinobisvanite phase exhibits a much higher photocatalytic activity due to its favourable band gap (2.4−2.5 eV) in the visible region of the electromagnetic spectrum (shows both visible light and UV absorption), and a valence band position suitable for driving water oxidation under illumination.[57]

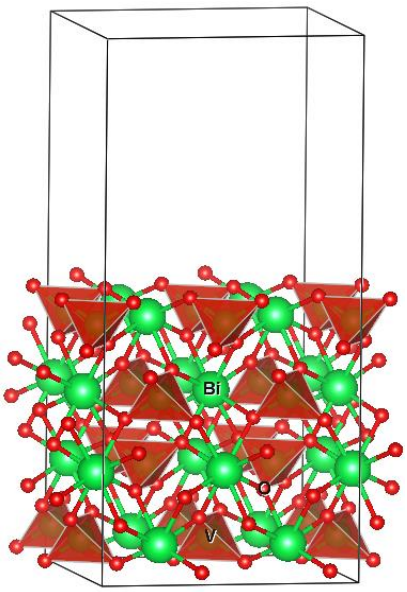

Figure 7. Optimized crystal structure of $BiVO_4$(001) slab.

The XRD analysis of our fabricated $BiVO_4$ films prove the formation of monoclinic clinobisvanite $BiVO_4$, so, that is why we have considered the same structure to investigate its theoretical insight. In order to correlate the experimental thin film properties, the [001] phase (generally, the more stable) is employed for simulations (Fig. 7).

Moreover, to analyze the electronic properties such as DOS/PDOS, band structure, the position of the valence band (VB) and conduction band (CB) are calculated from the optimized crystal structures. The DOS of $BiVO_4$(001) is simulated to find out it's band gap and edge positions which are given in Fig. 8. The simulated band gap of $BiVO_4$-001 is 2.25 eV which underestimate our experimental band gap (2.43 eV) to about 0.18 eV. This slight underestimation of the band gap is expected from LDA method of DFT calculation.[58]

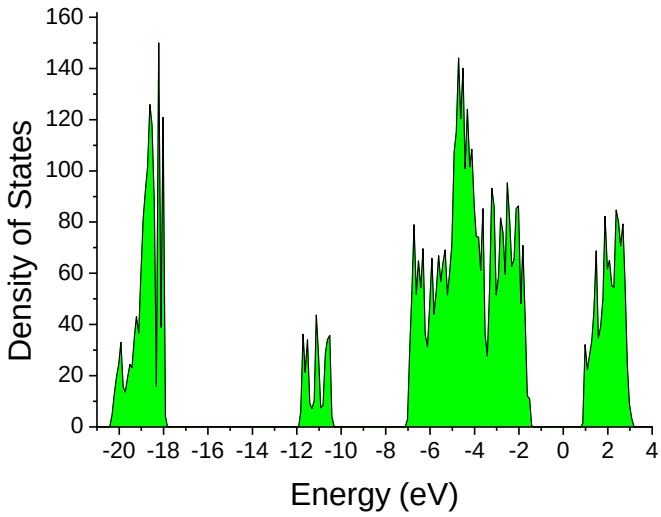

Figure 8: Total density of states of $BiVO_4$(001), the Fermi level is set to zero

In order to find the atomic and orbital contribution to form, valence, and conduction bands; the PDOS are simulated (Fig 9). In Fig. 9(a) the PDOS of $BiVO_4$(001) is shown, where the O atoms are responsible for the developing of valence band edge, however, the conduction band edge is populated by the atomic contribution of V atoms. Further details of the s, p, and d orbital contribution of Bi, V, and O are depicted in Fig. 9b-d. The PDOS of Bi atoms show that s

orbitals are involved in making the valence band edge of Bi while its p orbitals are situated in the conduction band edge. Both the valence and conduction bands of V atoms prominently consist of its 3d orbitals while in case of O, 2p orbitals have a major role in developing their band edge positions.

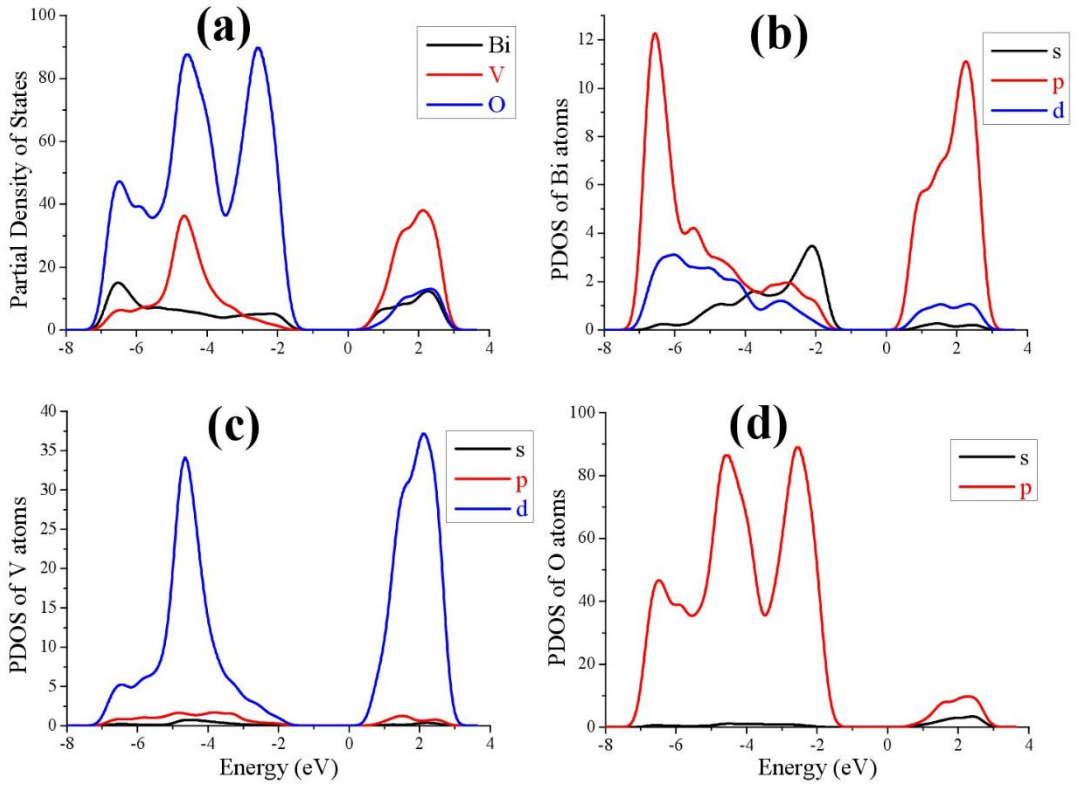

Figure 9: PDOS of $BiVO_4$(001) (a), Bi (b), V (c), and O (d); Fermi level is set to zero.

The valence band electronic structure of $BiVO_4$(001) spread over in the range of -0.65 to -19 eV, can be distinguished into three major parts (*vide infra*). The upper portion of the region from -0.65 eV to -6 eV is clearly dominated by the 2p orbitals of O, while its lower portion is partially hybridized by the d and s orbitals of V and Bi, respectively. The middle portion (-9 to -11 eV) of the valence band is equally occupied by sp of O, p d of V and sp orbitals of Bi. The region from -16 to -19 eV of the valence band is majorly contributed from the s orbital of O and its lower part is constituted from the hybridized s, p, and d orbitals of Bi and V atoms.

These orbitals have a major role in the developments of charge carriers and their effective masses.

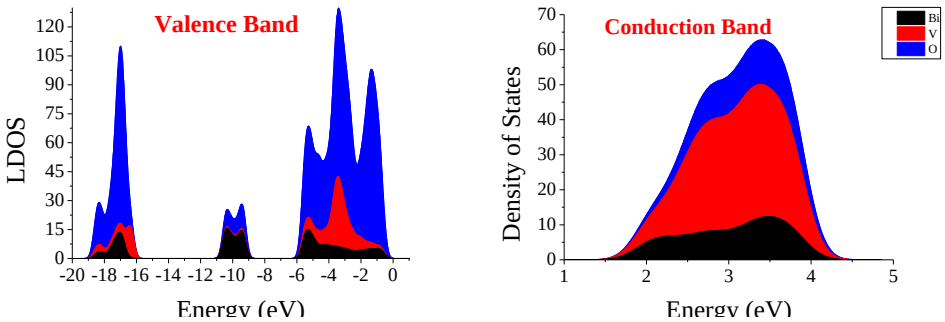

Figure 10: Valence and Conduction DOS of $BiVO_4$(001), Fermi level is set to zero

The conduction-band electronic structure is situated in the range of 1.60 to 4.4 eV, where the CBM is occupied by the d orbitals of V with the contribution of the p orbitals of Bi. The major portion of the unoccupied state within the conduction band of $BiVO_4$ is almost equally populated through the mutual hybridization of Bi p and V d orbitals. From Fig. 10, we can see that the anti-bonding orbitals of d and p of V and O are responsible for the effective masses of the electrons.

Band structure of the $BiVO_4$(001) along the k-points direction of Γ, Z, R, X, and M is given in Fig. 11. An indirect band gap of 2.25 eV is simulated which is in good agreement with the experimental and recently theoretical reported data[57]. Furthermore, this indirect band gap is due to the electronic excitation from the X→Γ, as clearly shown Fig. 11. Generally, in case of indirect band gap, the band edges are not aligned thus, the electron does not transit directly to the conduction band. In this process, both a photon and a phonon are involved. That is why a new concept of the mixed phases of the $BiVO_4$ is reported which can efficiently perform the water splitting.[59] At the Fermi energy of -5.73 eV, the vacuum phase VBM and CBM are ca. -6.38 and -4.13 eV, respectively. These simulated band edge energies indicate that $BiVO_4$ can be used as a photocatalytic material for redox reactions, such as water splitting but need

modification for high PEC performance. This statement clearly corroborates our photocatalytic activity (*vide infra*). The effective masses of the photogenerated electrons (m_e^*) and holes (m_h^*) along the X→Γ directions of k-points are calculated by fitting parabolic approximation around the bottom of the CBM or the top of the VBM, respectively; using equation 2 (Table 2):

$$m^* = \hbar^2 (d^2 E/dk^2)^{-1} \quad (2)$$

where $\hbar$ is the reduced Planck constant, E is the energy of an electron at wave vector k in the same band (VBM or CBM). To acquire the validity of the parabolic approximation within the specified space, the region for parabolic fitting is controlled by an energy difference of 1 meV along a particular direction around the VBM or CBM.

Table 2: Band gap and effective masses of photogenerated electrons and holes, estimated from the calculated band structure along the suitable direction.

Experimental	*Theoretical*	*Direction in Brillouin zone*	m_e^*/m_0	m_h^*/m_0	*Band gap*
$BiVO_4$ (Film)		Indirect			2.43
	$BiVO_4$(001)	**X→Γ**	**1.93**	**0.45**	**2.25**
Se Bulk		Direct			1.74
	Se Bulk	**Γ→ Γ**			**1.60**

The effective masses of electrons and holes of the $BiVO_4$(001) is calculated from the band structure as these photogenerated electrons and holes thermally relax to the bottom of the conduction band and the top of the valence band, respectively. The simulated values of the effective masses of photogenerated electrons and holes of the $BiVO_4$(001) slab are 0.45 and 1.93 m_e, respectively. Lighter mass of charge carriers the faster will be their movements at the interface.[60,61] Moreover, larger the difference between the effective mass of electron and hole the lower will their charge recombination. The lower photocatalytic activity of the

$BiVO_4$(001) is because of their heavy charge carriers. Our experimental results also support this theoretical observation.

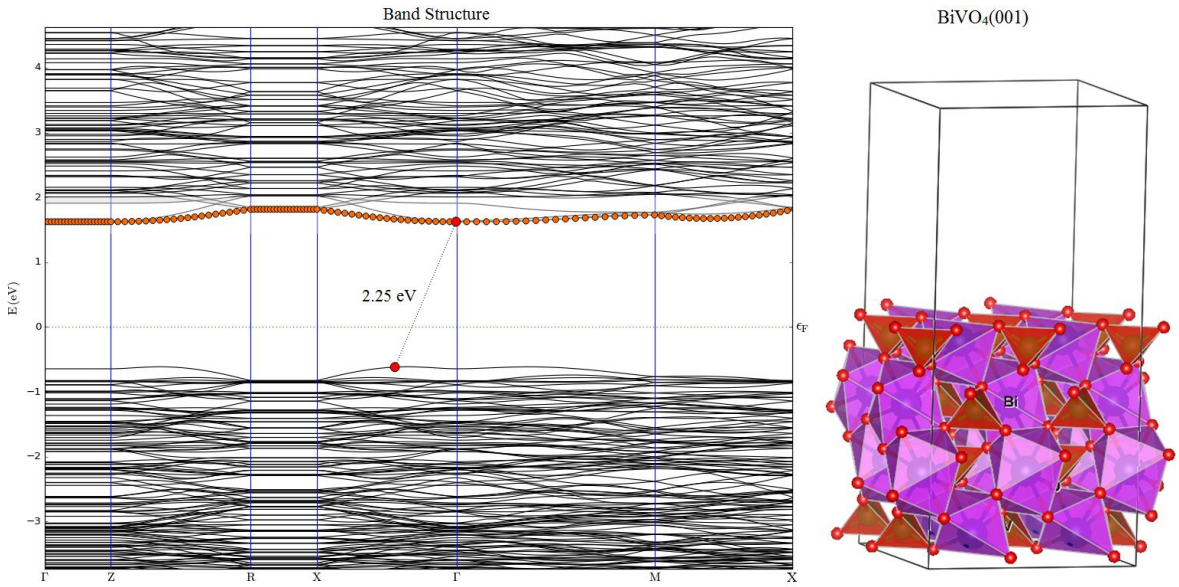

Figure 11: Band Structure of the $BiVO_4$ along the [001] direction; the Fermi level is set to zero.

The band structure of Se bulk along with its crystal structure is given in Fig 12, where the simulated band gap of 1.60 eV in the Γ→ Γ direction of the Brillouin zone has a nice correlation with our experimental observed of 1.74 eV. The vacuum simulated VBM and CBM of the Se bulk are ca. -5.08 and -3.48 eV, respectively at the Fermi energy of 4.22 eV.

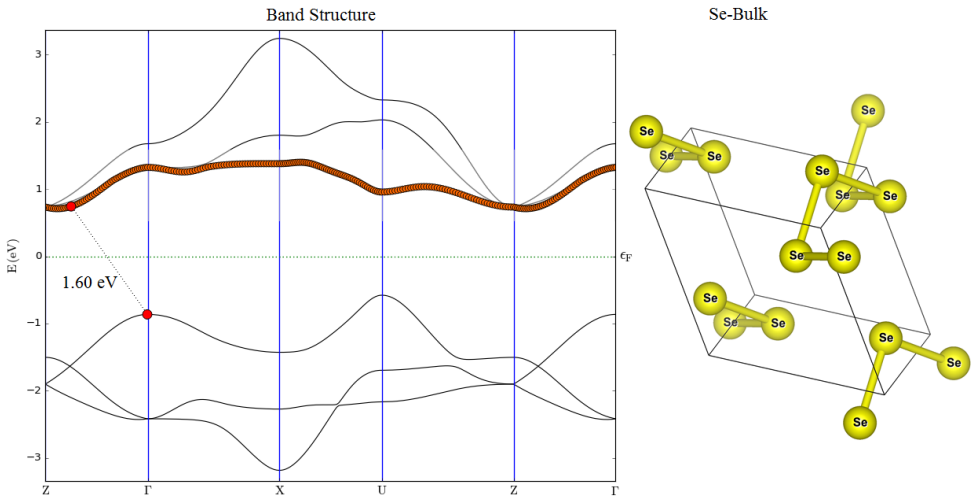

Figure 12. Band structure of the Se bulk, where the Fermi energy is set to zero.

As shown in Fig 13, the Se/$BiVO_4$ form a direct Z-scheme like heterojunction, where the enhanced photocurrent activities are because of Se layer. When light shines on Se/$BiVO_4$ heterostructure, the photogenerated electron of $BiVO_4$ in its CB recombine with a hole at VB of Se, consequences free electrons and at CB of Se case substentail increase in photocurrent as observed experimentally. This electron/hole recombination and separation create a direct Z-scheme like structure where the free electron at negative potential (CB) of Se is responsible for the enhancement of photocurrent (Fig 13).

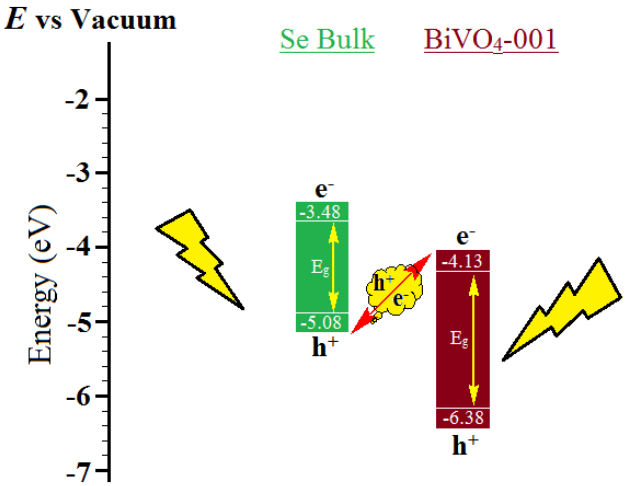

Figure 13. Energy level diagram of the simulated Se-bulk and $BiVO_4$(001)

3.6. Photoelectrochemical properties

The results of photocurrent density measurements are presented in Fig. 14 which is also compared with our previous work.[41] The photocurrent density obtained by the samples increase with increasing applied voltage. All samples of Se, $BiVO_4$, and Se/$BiVO_4$ show very good response under illumination and represent anodic photocurrent patterns which indicate that these electrodes have n-type semiconductor behavior. Moreover, the chopped photocurrent density-voltage is shown in Fig. 14b led us to conclude that Se/$BiVO_4$ photoanode is photocatalytically active under illumination. The photocurrent density of Se/$BiVO_4$ increased up to 2.2 $mAcm^{-2}$ at 1.3 V *vs*. SCE, much better than that of Se and $BiVO_4$. This enhanced photocurrent-density proves that Se could potentially be used in water splitting application as

an efficient complementary light absorbing layer with other metal oxides. This photocurrent enhancement might also be attributed to better charge transfer in heterojunction as well as reduction of the grains and particles size, observed from XRD and FESEM analysis. In general, the small grain and particle size enlarge the surface area for reaction. Hence, more surface area is exposed to the electrode/electrolyte interface which further promotes the photocatalytic process. Moreover, the porous structure of the Se/$BiVO_4$ film also widen the contact area between Se/$BiVO_4$ photoanode and electrolyte. This feature provides more surface sites for reaction, reducing charge transport distance and increase the accumulation of photogenerated electrons.[62-65]

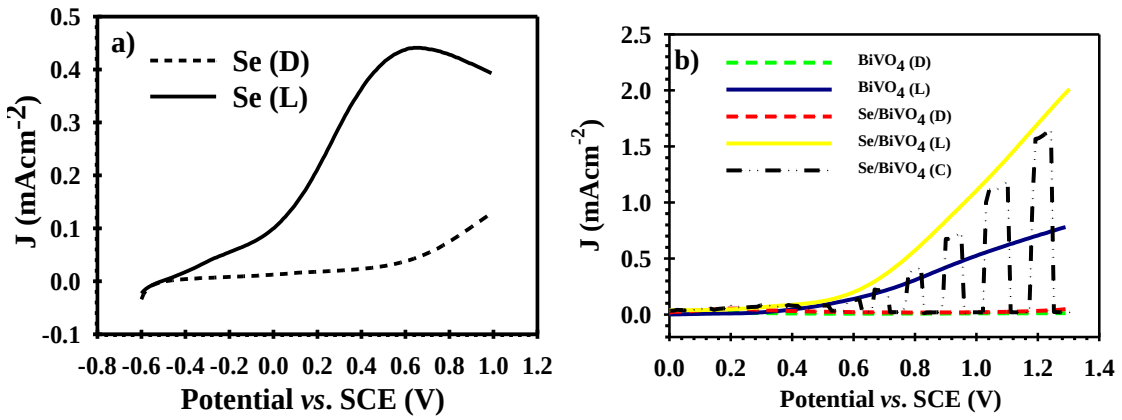

Figure 14: Photocurrent density of a) Se and (b) Se/$BiVO_4$ photoanodes under dark and light intensity of 100 $mWcm^{-2}$ in 0.5 M Na_2SO_4.

To further support the PEC enhancement of Se/$BiVO_4$, EIS measurement was carried out. Fig 15a shows the Nyquist plots of $BiVO_4$ and Se/$BiVO_4$, measured in 0.5 M Na_2SO_4 at 100 kHz to 0.1 Hz in the presence and absence of light (100 $mWcm^{-2}$) and 0.5 V applied potential *vs.* SCE. It can be seen that the diameter of curves diminished when the fabricated layers were exposed to light. The diameter of curves is a function of overall charge transfer through the electrodes. To quantify the charge transfer resistance, the EIS data were fitted to the equivalent circuit shown in the Fig. 15b. The equivalent electrical circuit consists of two relaxation times, dark and light condition. As observed in Fig. 15a, both loops in the equivalent circuit are in a

parallel configuration. The corresponding loop of the semiconductor (R_{SC} || CPE_{SC}) is in series with the interfacial resistance of the double layer/thin film (R_{dl}) and both of them are in parallel with the double layer capacitance (C_{dl}). For a more accurate representation of the capacitance behavior, the constant phase element (CPE) is used instead of a pure capacitor in the simulations. The impedance of a CPE (Z_{CPE}) for a non-ideal circuit element is given in equation 3:

$$Z_{CPE} = \frac{1}{Q(j2\pi f)^n} \quad (3)$$

Where f is applied frequency, j is imaginary number, $Q = C$ if the exponent n=1, and $Q \neq C$ if exponent $1 > n > 0$. It must be noted that the capacitance behavior is approximated by Q, if the electrode surface is rough or when the dielectric property of the electrode components is heterogeneous.[66] The detailed corresponding electro-kinetic elements for the samples are tabulated in Table 3. It is found that the charge transfers resistance of the semiconductor (R_{SC}) is in the order of $BiVO_4$ > $Se/BiVO_4$ in both light and dark conditions. The photocurrent-voltage curve (Fig. 14b) correlates with the EIS results. The smaller value of R_{SC} represents improved charge transport characteristics which provide favorable environment PEC reactions.[67]

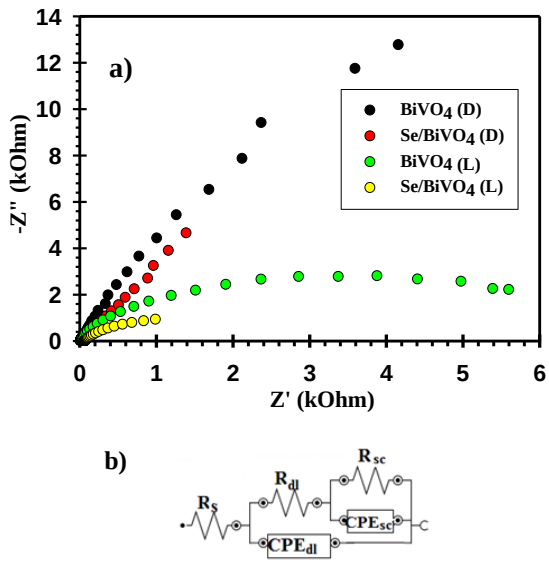

Figure 15: a) The Nyquist plots and b) equivalent circuit of $BiVO_4$ and $Se/BiVO_4$ photoanodes.

Table 3: The EIS parameters from the simulation of the equivalent circuit model at 0.5 V *vs*. SCE.

Electrode	R_S (Ω)	R_{dl} (kΩ)	C (μF)	R_{SC} (kΩ)	Q (Y_o) (μMho)	n
$BiVO_4$(L)	15.50	1.91	18.70	5.56	33.81	0.62
$BiVO_4$(D)	21.90	47.44	14.02	97.74	30.30	0.83
Se/$BiVO_4$(L)	26.30	5.93	120.60	2.24	717.00	0.84
Se/$BiVO_4$(D)	24.60	1.81	164.40	18.25	148.50	0.88

Figure S3 illustrates stability of Se/$BiVO_4$ electrode under chopped irradiation at 0.5 V *vs.* SCE in 0.5 M Na_2SO_4 with interval of 5 seconds. This potential was chosen because the photoelectrode has started to show response to the light at ~ 0.40 V. As noted in the figure, the photocurrent of the $BiVO_4$ film is gradually decreased with increasing illumination time, indicating the accumulation of the photo-generated holes at the surface of $BiVO_4$ due to poor kinetics charge transfer. However, the photocurrent value of 0.15 $mAcm^{-2}$ remains constant for 40 minutes for Se/$BiVO_4$. This constant photocurrent value confirms the photo-stability of the heterojunction film which can suggest that the Se is rather effective for improving the steady state PEC performance of $BiVO_4$ electrode. In the chopped stability plot, photocurrent spikes are observed, which indicate recombination. When the light is turned on, a sharp positive photocurrent spike is seen (which is termed the instantaneous hole current) which then decays to a steady state current after recombination of the holes with electrons.[69]

Figure 16a and b show the Mott-Schottky plot of Se and $BiVO_4$ electrodes that were measured in 0.5 M Na_2SO_4 electrolyte without illumination. The positive gradients of Mott-Schottky plots indicate the n-type semiconducting nature in which electrons are the majority charge carriers. The flat band potential, (E_{fb}) of Se electrode is estimated to be -0.17 V *vs*. SCE or equal to 0.074 V *vs*. NHE while, the E_{fb} of $BiVO_4$ is 0.33 V *vs*. SCE (0.57 V *vs*. NHE). At vacuum level, the CBM of Se is ca. -4.51 eV while that of $BiVO_4$ is -5.01 eV. By taking the

E_g of the Se electrode from Fig. 6b), the alignment of the energy levels for heterojunction Se/$BiVO_4$ can thus be drawn in Fig. 16c). Clearly, the valence band of Se is 1.814 V *vs*. NHE (-6.25 eV at vacuum). In a dual-absorber system (complementary absorption of UV-vis), electrons in both Se and $BiVO_4$ are excited upon illumination. It can be further concluded that most of the incidents light permeated through the $BiVO_4$ layer are absorbed by Se film. Due to the more negative potential of the conduction band of Se, photo-electrons at the conduction band of $BiVO_4$ recombined with holes at valence band of Se, which reduce the recombination of photogenerated electron-hole pairs by Se itself. This process generates more photocurrent since photo-generated electrons in the conduction band of Se are impeded to recombine with its holes. Note that, the high absorption intensity of Se/$BiVO_4$ electrode means more electron-hole pairs generation (Fig. 6a), does not contribute to the photo-oxidation process due to the thermodynamically forbidden hole transfer from Se to $BiVO_4$ (valence band Se located at more negative potential than valence band $BiVO_4$). However, this type of heterojunction had served as a center of charge recombination between holes in the valence band of Se and electrons from the conduction band of $BiVO_4$. As a result, this facilitates the accumulation of photo-generated electrons in Se to the external circuit and generates high photocurrent. This type of heterojunction was said to have more efficient charge separation and photocatalytic activities.[68]

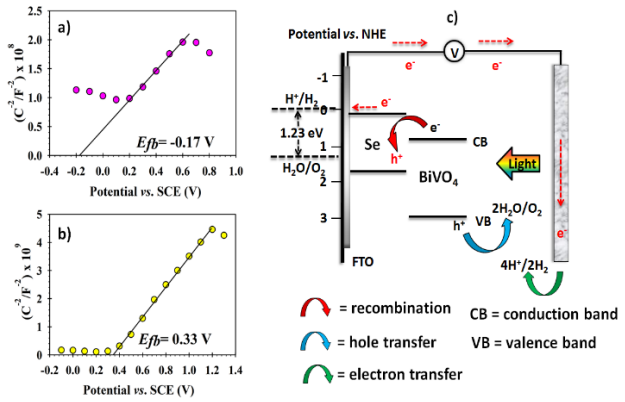

Figure 16: Mott-Schottky plots of a) Se and b) $BiVO_4$; c) the alignment of the energy levels of heterojunction Se/$BiVO_4$.

Conclusion

We have successfully fabricated a direct Z-scheme like heterojunction of Se and $BiVO_4$ (Se/$BiVO_4$), as a thin film for the improved PEC performance. The thin film photoanode are fully characterised by XRD, SEM, EDX, UV-Vis band gap calculations, PEC and electrochemical activity. Moreover, we also proposed band structure diagram for our heterojunction which is counterchecked by solid state theoretical simulations. The as-prepared Se and $BiVO_4$ exhibit monoclinic and monoclinic clinobisvanite structures, respectively and have low photocatalytic activities. An enhanced PEC activity is observed in case of heterojunction, compared to their individual constituents (Se and $BiVO_4$). Density functional theory (DFT) simulations are carried out for the $BiVO_4$ and Se to simulate their band gap, and band edge positions in the proposed heterojunction band diagram. The PEC properties of Se/$BiVO_4$ indicate that the increment in performance is due to the presence of Se layer which acts as a hole trapping agent, light absorber, and improves the charge separation in the resulted film. The Se/$BiVO_4$ has 1.5 times higher photocurrent density than that of $BiVO_4$ due to higher surface area, small grain size, high roughness, efficient charge separation and minimum charge recombination rate. Moreover, the existence of dual absorption layers of Se and $BiVO_4$ significantly increased the light absorption which has ultimately promoted more charge generation. The results prove that Se/$BiVO_4$ heterostructure is a potential candidate for PEC water splitting, confirmed by DFT simulations.

Acknowledgment

The authors would like to thank the National University of Malaysia for the financial support from grants GUP-2016-089. One of us (H.U) acknowledges the NOTUR supercomputing facilities within the project nn4608k.

References

(1) Crabtree, G. W.; Dresselhaus, M. S.; Buchanan, M. V. The Hydrogen Economy. *Phys. Today* **2004**, *57*, 39-44.
(2) Fujishima, A. Electrochemical Photolysis of Water at a Semiconductor Electrode. *Nature* **1972**, *238*, 37-38.
(3) Chen, X.; Shen, S.; Guo, L.; Mao, S. S. Semiconductor-Based Photocatalytic Hydrogen Generation. *Chem. Rev.* **2010**, *110*, 6503-6570.
(4) Grätzel, M. Photoelectrochemical Cells. *Nature* **2001**, *414*, 338-344.
(5) Williams, R. Becquerel Photovoltaic Effect in Binary Compounds. *J. Chem. Phys.* **1960**, *32*, 1505-1514.
(6) Ellis, A. B.; Kaiser, S. W.; Bolts, J. M.; Wrighton, M. S. Study of N-Type Semiconducting Cadmium Chalcogenide-Based Photoelectrochemical Cells Employing Polychalcogenide Electrolytes. *J. Am. Chem. Soc.* **1977**, *99*, 2839-2848.
(7) Tilley, S. D.; Cornuz, M.; Sivula, K.; Grätzel, M. Light-Induced Water Splitting with Hematite: Improved Nanostructure and Iridium Oxide Catalysis. *Angew. Chem. Int. Ed.* **2010**, *122*, 6549-6552.
(8) Sayama, K.; Nomura, A.; Zou, Z.; Abe, R.; Abe, Y.; Arakawa, H. Photoelectrochemical Decomposition of Water on Nanocrystalline Bivo 4 Film Electrodes under Visible Light. *Chem. Commun.* **2003**, 2908-2909.
(9) Hong, S. J.; Lee, S.; Jang, J. S.; Lee, J. S. Heterojunction Bivo 4/Wo 3 Electrodes for Enhanced Photoactivity of Water Oxidation. *Energy & Envir. Sci.* **2011**, *4*, 1781-1787.
(10) Su, J.; Guo, L.; Bao, N.; Grimes, C. A. Nanostructured Wo3/Bivo4 Heterojunction Films for Efficient Photoelectrochemical Water Splitting. *Nano Lett.* **2011**, *11*, 1928-1933.
(11) Saito, R.; Miseki, Y.; Sayama, K. Highly Efficient Photoelectrochemical Water Splitting Using a Thin Film Photoanode of Bivo 4/Sno 2/Wo 3 Multi-Composite in a Carbonate Electrolyte. *Chem. Commun.* **2012**, *48*, 3833-3835.
(12) Saito, R.; Miseki, Y.; Sayama, K. Photoanode Characteristics of Multi-Layer Composite Bivo 4 Thin Film in a Concentrated Carbonate Electrolyte Solution for Water Splitting. *J. Photochem. Photobiol A: Chem.* **2013**, *258*, 51-60.
(13) Krysa, J.; Zlamal, M.; Kment, S.; Brunclikova, M.; Hubicka, Z. Tio2 and Fe2o3 Films for Photoelectrochemical Water Splitting. *Molecules* **2015**, *20*, 1046-1058.
(14) Xie, B.; Zhang, H.; Cai, P.; Qiu, R.; Xiong, Y. Simultaneous Photocatalytic Reduction of Cr (Vi) and Oxidation of Phenol over Monoclinic Bivo 4 under Visible Light Irradiation. *Chemosphere* **2006**, *63*, 956-963.
(15) Tokunaga, S.; Kato, H.; Kudo, A. Selective Preparation of Monoclinic and Tetragonal Bivo4 with Scheelite Structure and Their Photocatalytic Properties. *Chem. Mater.* **2001**, *13*, 4624-4628.
(16) Abdi, F. F.; van de Krol, R. Nature and Light Dependence of Bulk Recombination in Co-Pi-Catalyzed Bivo4 Photoanodes. *J. Phys. Chem. C* **2012**, *116*, 9398-9404.
(17) Yao, W.; Iwai, H.; Ye, J. Effects of Molybdenum Substitution on the Photocatalytic Behavior of Bivo 4. *Dalton Trans.* **2008**, 1426-1430.
(18) Abdi, F. F.; Firet, N.; van de Krol, R. Efficient Bivo4 Thin Film Photoanodes Modified with Cobalt Phosphate Catalyst and W-Doping. *ChemCatChem* **2013**, *5*, 490-496.

(19) Jeong, H. W.; Jeon, T. H.; Jang, J. S.; Choi, W.; Park, H. Strategic Modification of Bivo4 for Improving Photoelectrochemical Water Oxidation Performance. *J. Phys. Chem. C* **2013**, *117*, 9104-9112.
(20) Zhong, D. K.; Choi, S.; Gamelin, D. R. Near-Complete Suppression of Surface Recombination in Solar Photoelectrolysis by "Co-Pi" Catalyst-Modified W: Bivo4. *J. Am. Chem. Soc.* **2011**, *133*, 18370-18377.
(21) Jia, Q.; Iwashina, K.; Kudo, A. Facile Fabrication of an Efficient Bivo4 Thin Film Electrode for Water Splitting under Visible Light Irradiation. *Proc. Natl. Acad. Sci. U.S.A.* **2012**, *109*, 11564-11569.
(22) Seabold, J. A.; Choi, K.-S. Efficient and Stable Photo-Oxidation of Water by a Bismuth Vanadate Photoanode Coupled with an Iron Oxyhydroxide Oxygen Evolution Catalyst. *J. Am. Chem. Soc.* **2012**, *134*, 2186-2192.
(23) Ding, C.; Shi, J.; Wang, D.; Wang, Z.; Wang, N.; Liu, G.; Xiong, F.; Li, C. Visible Light Driven Overall Water Splitting Using Cocatalyst/Bivo 4 Photoanode with Minimized Bias. *Phys. Chem. Chem. Phys.* **2013**, *15*, 4589-4595.
(24) Chatchai, P.; Murakami, Y.; Kishioka, S.-y.; Nosaka, A.; Nosaka, Y. Fto⁄ Sno2⁄ Bivo4 Composite Photoelectrode for Water Oxidation under Visible Light Irradiation. *Electrochem. Solid-State. Lett.* **2008**, *11*, H160-H163.
(25) Li, J.; Wu, N. Semiconductor-Based Photocatalysts and Photoelectrochemical Cells for Solar Fuel Generation: A Review. *Catal. Sci. Technol.* **2015**, *5*, 1360-1384.
(26) Lou, Z.; Li, F.; Deng, J.; Wang, L.; Zhang, T. Branch-Like Hierarchical Heterostructure (A-Fe2o3/Tio2): A Novel Sensing Material for Trimethylamine Gas Sensor. *ACS Appl. Mater. Interfac.* **2013**, *5*, 12310-12316.
(27) An, X.; Li, T.; Wen, B.; Tang, J.; Hu, Z.; Liu, L. M.; Qu, J.; Huang, C.; Liu, H. New Insights into Defect-Mediated Heterostructures for Photoelectrochemical Water Splitting. *Adv. Energy Mater.* **2016**.
(28) Dong, F.; Zhao, Z.; Xiong, T.; Ni, Z.; Zhang, W.; Sun, Y.; Ho, W.-K. In Situ Construction of G-C3n4/G-C3n4 Metal-Free Heterojunction for Enhanced Visible-Light Photocatalysis. *ACS Appl. Mater. Interfac.* **2013**, *5*, 11392-11401.
(29) Mali, M. G.; Yoon, H.; Kim, M.-w.; Swihart, M. T.; Al-Deyab, S. S.; Yoon, S. S. Electrosprayed Heterojunction Wo3/Bivo4 Films with Nanotextured Pillar Structure for Enhanced Photoelectrochemical Water Splitting. *Appl. Phys. Lett.* **2015**, *106*, 151603.
(30) Pihosh, Y.; Turkevych, I.; Mawatari, K.; Uemura, J.; Kazoe, Y.; Kosar, S.; Makita, K.; Sugaya, T.; Matsui, T.; Fujita, D. Photocatalytic Generation of Hydrogen by Core-Shell Wo3/Bivo4 Nanorods with Ultimate Water Splitting Efficiency. *Sci. Rep.* **2015**, *5*.
(31) Jung, H.; Chae, S. Y.; Shin, C.; Min, B. K.; Joo, O.-S.; Hwang, Y. J. Effect of the Si/Tio2/Bivo4 Heterojunction on the Onset Potential of Photocurrents for Solar Water Oxidation. *ACS Appl. Mater. Interfaces* **2015**, *7*, 5788-5796.
(32) Yu, H.; Chen, S.; Quan, X.; Zhao, H.; Zhang, Y. Silicon Nanowire/Tio 2 Heterojunction Arrays for Effective Photoelectrocatalysis under Simulated Solar Light Irradiation. *Appl. Catal. B-Environ* **2009**, *90*, 242-248.
(33) Hwang, Y. J.; Boukai, A.; Yang, P. High Density N-Si/N-Tio2 Core/Shell Nanowire Arrays with Enhanced Photoactivity. *Nano Lett.* **2008**, *9*, 410-415.
(34) Catchpole, K.; Mc Cann, M.; Blakers, A.; Weber, K. In *Proceedings 16th European Photovoltaic Solar Energy Conference* 2000, p 1165-1168.
(35) Nath, S.; Ghosh, S. K.; Panigahi, S. Synthesis of Selenium Nanoparticle and Its Photocatalytic Application for Decolorization of Methylene Blue under Uv Irradiation. **2004**.
(36) Yang, L.; Shen, Y.; Xie, A.; Liang, J.; Zhang, B. Synthesis of Se Nanoparticles by Using Tsa Ion and Its Photocatalytic Application for Decolorization of Cango Red under Uv Irradiation. *Mater. Res. Bull.* **2008**, *43*, 572-582.

(37) Johnson, J.; Saboungi, M.-L.; Thiyagarajan, P.; Csencsits, R.; Meisel, D. Selenium Nanoparticles: A Small-Angle Neutron Scattering Study. *J. Phys. Chem. B* **1999**, *103*, 59-63.
(38) Ebadi, M.; Sulaiman, M. Y.; Mat-Teridi, M. A.; Basirun, W. J.; Golsefidi, M. A.; Sopian, K.; Sateei, A.; Mehrabian, R. Z. Efficient Photo-Electrochemical Performance Using Cuo-Based Electrodes in Aqua Medium. *J. Appl. Electrochem.* **2016**, *46*, 645-653.
(39) Ito, H.; Oka, M.; Ogino, T.; Takeda, A.; Mizushima, Y. Selenium Thin Film Solar Cell. *Jap. J. Appl. Phys.* **1982**, *21*, 77.
(40) Luo, C.; Xu, Y.; Zhu, Y.; Liu, Y.; Zheng, S.; Liu, Y.; Langrock, A.; Wang, C. Selenium@ Mesoporous Carbon Composite with Superior Lithium and Sodium Storage Capacity. *ACS Nano* **2013**, *7*, 8003-8010.
(41) Mohd-Nasir, S.; Mat-Teridi, M.; Ebadi, M.; Sagu, J.; Sulaiman, M. Y.; Ludin, N. A.; Ibrahim, M. Influence of Ethylene Glycol on Efficient Photoelectrochemical Activity of Bivo4 Photoanode Via Aacvd. *Phys. Status Solidi A* **2015**, *212*, 2910-2914.
(42) Giannozzi, P.; Baroni, S.; Bonini, N.; Calandra, M.; Car, R.; Cavazzoni, C.; Ceresoli, D.; Chiarotti, G. L.; Cococcioni, M.; Dabo, I. Quantum Espresso: A Modular and Open-Source Software Project for Quantum Simulations of Materials. *Phys. Condens. Matter* **2009**, *21*, 395502.
(43) Momma, K.; Izumi, F. An Integrated Three-Dimensional Visualization System Vesta Using Wxwidgets. *Commision Crystallogr. Comput., IUCr Newslett* **2006**, 106-119.
(44) VirtualNanoLab. *QuantumWise A/S (www.quantumwise.com)* **2016**, *2.1*.
(45) Sleight, A.; Chen, H.-Y.; Ferretti, A.; Cox, D. Crystal Growth and Structure of Bivo 4. *Mater. Res. Bull.* **1979**, *14*, 1571-1581.
(46) Xi, G.; Ye, J. Synthesis of Bismuth Vanadate Nanoplates with Exposed {001} Facets and Enhanced Visible-Light Photocatalytic Properties. *Chem. Commun.* **2010**, *46*, 1893-1895.
(47) Press, W. H. *Numerical Recipes 3rd Edition: The Art of Scientific Computing*; Cambridge university press, 2007.
(48) Pilli, S. K.; Janarthanan, R.; Deutsch, T. G.; Furtak, T. E.; Brown, L. D.; Turner, J. A.; Herring, A. M. Efficient Photoelectrochemical Water Oxidation over Cobalt-Phosphate (Co-Pi) Catalyst Modified Bivo 4/1d-Wo 3 Heterojunction Electrodes. *Phys. Chem. Chem. Phys.* **2013**, *15*, 14723-14728.
(49) Jiang, J.; Wang, M.; Li, R.; Ma, L.; Guo, L. Fabricating Cds/Bivo 4 and Bivo 4/Cds Heterostructured Film Photoelectrodes for Photoelectrochemical Applications. *Int. J. Hydrogen Energy* **2013**, *38*, 13069-13076.
(50) Najib áYahya, M. K.; áMohamad Sapian, N. W.; Ludin, N.; AdibáIbrahim, M.; Teridi, M. A. Heterojunction Cr2o3/Cuo: Ni Photocathodes for Enhanced Photoelectrochemical Performance. *RSC Adv.* **2016**.
(51) Cooper, J. K.; Gul, S.; Toma, F. M.; Chen, L.; Liu, Y.-S.; Guo, J.; Ager, J. W.; Yano, J.; Sharp, I. D. Indirect Bandgap and Optical Properties of Monoclinic Bismuth Vanadate. *J. Phys. Chem. C* **2015**, *119*, 2969-2974.
(52) Wang, K.; Shi, Y.; Zhang, H.; Xing, Y.; Dong, Q.; Ma, T. Selenium as a Photoabsorber for Inorganic–Organic Hybrid Solar Cells. *Phys. Chem. Chem. Phys.* **2014**, *16*, 23316-23319.
(53) Rossell, M. D.; Agrawal, P.; Borgschulte, A.; Hébert, C. c.; Passerone, D.; Erni, R. Direct Evidence of Surface Reduction in Monoclinic Bivo4. *Chem. Mater.* **2015**, *27*, 3593-3600.
(54) Morgan, B. J.; Watson, G. W. A Density Functional Theory+ U Study of Oxygen Vacancy Formation at the (110),(100),(101), and (001) Surfaces of Rutile Tio2. *J. Phys. Chem. C* **2009**, *113*, 7322-7328.
(55) Pan, J.; Liu, G.; Lu, G. Q. M.; Cheng, H. M. On the True Photoreactivity Order of {001},{010}, and {101} Facets of Anatase Tio2 Crystals. *Angew. Chem. Inter. Ed.* **2011**, *50*, 2133-2137.

(56) Batzill, M. Fundamental Aspects of Surface Engineering of Transition Metal Oxide Photocatalysts. *Energy & Environ. Sci.* **2011**, *4*, 3275-3286.
(57) Park, H. S.; Kweon, K. E.; Ye, H.; Paek, E.; Hwang, G. S.; Bard, A. J. Factors in the Metal Doping of Bivo4 for Improved Photoelectrocatalytic Activity as Studied by Scanning Electrochemical Microscopy and First-Principles Density-Functional Calculation. *J. Phys. Chem. C* **2011**, *115*, 17870-17879.
(58) Tran, F.; Blaha, P. Accurate Band Gaps of Semiconductors and Insulators with a Semilocal Exchange-Correlation Potential. *Phys. Rev. Lett.* **2009**, *102*, 226401.
(59) Tan, H. L.; Wen, X.; Amal, R.; Ng, Y. H. Bivo4 {010} and {110} Relative Exposure Extent: Governing Factor of Surface Charge Population and Photocatalytic Activity. *J. Phys. Chem. Lett.* **2016**, *7*, 1400-1405.
(60) Giorgi, G.; Fujisawa, J.-I.; Segawa, H.; Yamashita, K. Small Photocarrier Effective Masses Featuring Ambipolar Transport in Methylammonium Lead Iodide Perovskite: A Density Functional Analysis. *J. Phys. Chem. Lett.* **2013**, *4*, 4213-4216.
(61) Zhang, J.; Wageh, S.; Al-Ghamdi, A.; Yu, J. New Understanding on the Different Photocatalytic Activity of Wurtzite and Zinc-Blende Cds. *Appl. Catal. B: Environ.* **2016**, *192*, 101-107.
(62) Xu, C.; Shin, P.; Cao, L.; Gao, D. Preferential Growth of Long Zno Nanowire Array and Its Application in Dye-Sensitized Solar Cells. *J. Phys. Chem. C* **2009**, *114*, 125-129.
(63) Shi, J.; Hara, Y.; Sun, C.; Anderson, M. A.; Wang, X. Three-Dimensional High-Density Hierarchical Nanowire Architecture for High-Performance Photoelectrochemical Electrodes. *Nano Lett.* **2011**, *11*, 3413-3419.
(64) Cho, I. S.; Chen, Z.; Forman, A. J.; Kim, D. R.; Rao, P. M.; Jaramillo, T. F.; Zheng, X. Branched Tio2 Nanorods for Photoelectrochemical Hydrogen Production. *Nano Lett.* **2011**, *11*, 4978-4984.
(65) Xu, C.; Wu, J.; Desai, U. V.; Gao, D. Multilayer Assembly of Nanowire Arrays for Dye-Sensitized Solar Cells. *J. Am. Chem. Soc.* **2011**, *133*, 8122-8125.
(66) Chen, Z.; Dinh, H. N.; Miller, E. Photoelectrochemical Water Splitting. *SpringerBriefs in Energy, New York* **2013**, 49-61.
(67) Jo, W. J.; Jang, J. W.; Kong, K. j.; Kang, H. J.; Kim, J. Y.; Jun, H.; Parmar, K.; Lee, J. S. Phosphate Doping into Monoclinic Bivo4 for Enhanced Photoelectrochemical Water Oxidation Activity. *Angew. Chem. Int. Ed.* **2012**, *51*, 3147-3151.
(68) Li, J.; Wu, N. Semiconductor-Based Photocatalysts and Photoelectrochemical Cells for Solar Fuel Generation: A Review. *Catal. Sci. & Technol.* **2015**, *5*, 1360-1384.
(69) Pihosh, Y.; Turkevych, I.; Mawatari, K.; Asai, T.; Hisatomi, T.; Uemura, J.; Tosa, M.; Shimamura, K.; Kubota, J.; Domen, K.; Kitamori, T. Nanostructured $WO_3/BiVO_4$ photoanodes for efficient photoelectrochemical water splitting. *Small*, **2014**, *10*, 3692-3699.